

Epidemic Transmission Modeling with Fractional Derivatives and Environmental Pathogens

Moein Khalighi^b, Faiçal Ndairou^a, Leo Lahti^{b,*}

^a*Institute of Mathematics and Informatics, Bulgarian Academy of Sciences, Bulgaria, Sofia 1113, ul. Akad. G. Bonchev, bl. 8*

^b*Department of Computing, Faculty of Technology, University of Turku*

Abstract

This research presents an advanced fractional-order compartmental model designed to delve into the complexities of COVID-19 transmission dynamics, specifically accounting for the influence of environmental pathogens on disease spread. By enhancing the classical compartmental framework, our model distinctively incorporates the effects of order derivatives and environmental shedding mechanisms on the basic reproduction numbers, thus offering a holistic perspective on transmission dynamics. Leveraging fractional calculus, the model adeptly captures the memory effect associated with disease spread, providing an authentic depiction of the virus's real-world propagation patterns. A thorough mathematical analysis confirming the existence, uniqueness, and stability of the model's solutions emphasizes its robustness. Furthermore, the numerical simulations, meticulously calibrated with real COVID-19 case data, affirm the model's capacity to emulate observed transmission trends, demonstrating the pivotal role of environmental transmission vectors in shaping public health strategies. The study highlights the critical role of environmental sanitation and targeted interventions in controlling the pandemic's spread, suggesting new insights for research and policy-making in infectious disease management.

Keywords: mathematical modeling of COVID-19 pandemics, pathogens, environmental effect, fractional differential equations, numerical simulations.

2010 MSC: 26A33, 34A08, 92D30.

1. Introduction

A comprehensive understanding of the disease transmission dynamics is essential to control the spread of epidemic diseases and prevent future viral outbreaks. Many advanced mathematical models have been developed to describe the spread of the virus. In this context, various incidence functions exist to model virus mutations during infection when infectious individuals' dynamics change. Examples include the bilinear incidence or law of mass action described in [1] and [2], the saturated incidence function in [3] and [4], and the Beddington–DeAngelis function in [5] and [6]. Other specific nonlinear incidence functions are also used in [7] and [8], and recent developments in this field suggest utilizing Stieltjes derivatives to model time-varying contact rates and other parameters [9].

The existing models for studying disease transmission have faced limitations due to their simplistic assumptions of uniform interactions among individuals. Such models overlook the intricate dynamics involved in disease spread, including the transmission via contaminated environments and the movement of live viruses. To address these shortcomings, recent research has proposed new modeling approaches that include environmental pathogens [10, 11, 12], showing promise in

*Corresponding author.

Email addresses: moein.khalighi@utu.fi (Moein Khalighi), faical@math.bas.bg (Faiçal Ndairou), leo.lahti@utu.fi (Leo Lahti)

capturing more realistic disease dynamics. However, these advanced models often struggle to fit real-world data accurately, partly because they omit critical factors such as mortality due to the virus [10]. Furthermore, the application of fractional calculus, an area with significant potential for improving model accuracy, has not been thoroughly explored in this context.

Fractional calculus represents a novel method that enhances disease transmission models by integrating memory effects and long-range dependencies [13, 14, 15, 16]. This approach, by using incommensurate fractional derivatives, offers enhanced flexibility, enabling the models to more accurately reflect the complex and diverse nature of disease spread [17, 18]. This complexity encompasses varying demographics, social behaviors, and intervention strategies that influence transmission rates. Despite the application of fractional order derivatives in modeling disease dynamics with considerations for environmental factors and social distancing measures, challenges remain regarding the mathematical precision and reliability of critical indicators, such as the basic reproduction number, R_0 [13].

In our research, we tackle these challenges by ensuring precise computation of R_0 and affirming the local and global stability of the disease-free equilibrium. We incorporate incommensurate fractional order derivatives into ordinary differential equations (ODEs) to enhance the depiction of memory effects. This improvement aims to develop a more flexible model for assessing how past infections influence future disease transmission. Our model also includes deceased compartments. This work delves into the existence, uniqueness, and boundedness of the system's solutions within the fractional framework. Notably, in our fractional model, the value of R_0 is also influenced by the derivative order, providing a more detailed and accurate understanding of disease transmission dynamics. Furthermore, we conduct a comparative analysis of R_0 in scenarios with and without environmental pathogens, considering both integer and fractional order models, to underline the critical role of environmental transmission pathways.

The article is organized as follows: In Section 2, we introduce the structure of our model. It features Caputo fractional derivatives and delineates various population classes—susceptible, exposed, symptomatic, and asymptomatic infectious individuals, those in recovery, fatalities, and a compartment for environmental pathogens, each with its respective coefficients. Section 3 delves into the mathematical analysis of the model. Here, we explore the existence and uniqueness of solutions, their boundedness, the derivation of the basic reproduction number, and an examination of the disease-free equilibrium to assess both local and global stability. Section 4 presents the numerical findings, including the fitting of the model to real data from South Africa. Additionally, sensitivity analysis is performed to evaluate the effect of various model parameters and order of derivatives on the basic reproduction number, which offers valuable insights for controlling the spread of COVID-19.

2. The fractional-order model

This section presents a modified fractional compartmental model for COVID-19, building upon the framework originally proposed by [10]. The following system of equations describes the model:

$$\left\{ \begin{array}{l}
{}^C D_{0+}^{\alpha_S} S(t) = \Lambda^{\alpha_S} - \frac{\beta_1^{\alpha_S} S(t)W(t)}{1 + \phi_1 W(t)} - \frac{\beta_2^{\alpha_S} S(t)(I_A(t) + I_S(t))}{1 + \phi_2 (I_A(t) + I_S(t))} + \psi^{\alpha_S} E(t) - \mu^{\alpha_S} S(t), \\
{}^C D_{0+}^{\alpha_E} E(t) = \frac{\beta_1^{\alpha_E} S(t)W(t)}{1 + \phi_1 W(t)} + \frac{\beta_2^{\alpha_E} S(t)(I_A(t) + I_S(t))}{1 + \phi_2 (I_A(t) + I_S(t))} - \psi^{\alpha_E} E(t) - \mu^{\alpha_E} E(t) - \omega^{\alpha_E} E(t), \\
{}^C D_{0+}^{\alpha_{I_A}} I_A(t) = (1 - \delta)\omega^{\alpha_{I_A}} E(t) - (\mu^{\alpha_{I_A}} + \sigma^{\alpha_{I_A}})I_A(t) - \gamma_A^{\alpha_{I_A}} I_A(t), \\
{}^C D_{0+}^{\alpha_{I_S}} I_S(t) = \delta\omega^{\alpha_{I_S}} E(t) - (\mu^{\alpha_{I_S}} + \sigma^{\alpha_{I_S}})I_S(t) - \gamma_S^{\alpha_{I_S}} I_S(t), \\
{}^C D_{0+}^{\alpha_R} R(t) = \gamma_S^{\alpha_R} I_S(t) + \gamma_A^{\alpha_R} I_A(t) - \mu^{\alpha_R} R(t), \\
{}^C D_{0+}^{\alpha_D} D(t) = \sigma^{\alpha_D} (I_S(t) + I_A(t)) - \mu^{\alpha_D} D(t), \\
{}^C D_{0+}^{\alpha_W} W(t) = \eta_A^{\alpha_W} I_A(t) + \eta_S^{\alpha_W} I_S(t) - \mu_P^{\alpha_W} W(t).
\end{array} \right. \quad (1)$$

The model delineates the dynamics of COVID-19 across seven distinct compartments, representing the stages of the disease from susceptibility to recovery or death, alongside the environmental presence of pathogens. These compartments are denoted as follows: Susceptible individuals (S), Exposed individuals (E), Asymptomatic infectious individuals (I_A), Symptomatic infectious individuals (I_S), Recovered individuals (R), Deceased individuals (D), and Environmental pathogens (W). Detailed parameter descriptions are provided in Table 1.

Table 1: Description of the parameters and their units.

Parameter	Description	Unit
Λ	Rate of new susceptible births per day	1/days
μ	Daily per capita death rate, excluding disease deaths	1/days
μ_P	Daily death rate of pathogens in the environment	1/days
ϕ_1	Fraction interacting with infectious environments daily	-
ϕ_2	Fraction interacting with infectious individuals daily	-
β_1	Daily infection rate, S to E , via environmental contact	1/days
β_2	Daily infection rate, S to E , via contact with I_A or I_S	1/days
δ	Fraction of symptomatic infectious people	-
ψ	Daily rate of E to S due to immune response	1/days
ω	Daily progression rate from E to I_A or I_S	1/days
σ	Daily disease mortality rate	1/days
γ_S	Daily recovery rate of symptomatic individuals	1/days
γ_A	Daily recovery rate of asymptomatic individuals	1/days
η_S	Daily virus spread rate to environment by I_S	1/days
η_A	Daily virus spread rate to environment by I_A	1/days

In our model, Caputo fractional-order derivatives are employed to capture the complex dynamics of the disease's spread, with a formal definition provided in the subsequent section. It is important to note that all model parameters, except for ϕ_1 , ϕ_2 , and δ , possess dimensions of $1/t^{\alpha_i}$ (where i represents the different compartments: S , E , I_A , I_S , R , D , W). To ensure dimensional consistency, as stressed by [19], these parameters are exponentiated to their respective derivative orders. This approach not only adheres to the mathematical rigor required for the model's integrity but also enhances its applicability in capturing the behaviors of disease transmission and progression.

The infection transmission mechanisms, represented by $\frac{\beta_1^{\alpha_S} SW}{1 + \phi_1 W}$, $\frac{\beta_2^{\alpha_S} S(I_A + I_S)}{1 + \phi_2 (I_A + I_S)}$, integrate the concept of saturation in incidence functions, reflecting a reduction in infection rates as a result of social distancing and other behavioral adjustments ([20, 21, 22, 23]). This approach, validated

by [10] and further explored by [24], expresses the interplay between population behavior and the spread of the disease. In our proposed model, we have also incorporated the dynamics of deceased individuals, D , an aspect not covered in the original model [10]. This enhancement allows for a more plausible fit with the available data.

3. Mathematical analysis of the model

3.1. Preliminaries

This section covers key concepts from fractional calculus, including the Riemann-Liouville fractional integral, Caputo fractional derivative operator, and Mittag-Leffler function [25, 26].

We denote the time-fractional Caputo derivative of order $\alpha \in \mathbb{R}^+$, starting from the initial time $t = 0$, as ${}^C D_{0+}^\alpha$. For a continuously differentiable function f , the Caputo fractional derivative at time t is given by:

$${}^C D_{0+}^\alpha f(t) = I_{0+}^{m-\alpha} f^{(m)}(t) = \frac{1}{\Gamma(m-\alpha)} \int_0^t \frac{f^{(m)}(\tau) d\tau}{(t-\tau)^{1+\alpha-m}}, \quad (2)$$

where $f^{(m)}(t)$ signifies the m -th order derivative of $f(t)$, with m being the smallest integer not less than α . For the scope of this study, considering $0 < \alpha \leq 1$, it follows that $m = 1$. The operator $I_{0+}^{1-\alpha}$ represents the Riemann-Liouville fractional integral of order $1 - \alpha$, defined as

$$I_{0+}^\alpha f(t) = \frac{1}{\Gamma(\alpha)} \int_0^t \frac{f(\tau) d\tau}{(t-\tau)^{1-\alpha}}, \quad (3)$$

with Γ denoting the gamma function.

The Mittag-Leffler function plays a crucial role in our discussion. This function is useful for its properties in fractional calculus and its applications. In this study, we use an asymptotic expansion of this function defined as follows:

$$E_{\alpha,\beta}(z) \approx - \sum_{k=1}^N \frac{z^{-k}}{\Gamma(\beta - \alpha k)} + O\left(\frac{1}{|z|^{1+N}}\right),$$

for large values of $|z|$ (specifically, as $|z|$ approaches infinity), and when the argument of z ($|\arg(z)|$) is between $\frac{\alpha\pi}{2}$ and π . The notation $O\left(\frac{1}{|z|^{1+N}}\right)$ indicates the asymptotic behavior of the function as $|z|$ becomes very large, providing insight into how the function decays over large distances or times [27].

3.2. Existence and Uniqueness

This section delves into the theoretical foundation concerning the existence and uniqueness of solutions for the system outlined in Equation 1, leveraging the principles of fixed-point theory and the Picard-Lindelöf theorem [28]. We reformulate system 1 as follows:

$$\begin{cases} {}^C D_{0+}^{\alpha_S} S(t) = F_1(t, S), \\ {}^C D_{0+}^{\alpha_E} E(t) = F_2(t, E), \\ {}^C D_{0+}^{\alpha_{I_A}} I_A(t) = F_3(t, I_A), \\ {}^C D_{0+}^{\alpha_{I_S}} I_S(t) = F_4(t, I_S), \\ {}^C D_{0+}^{\alpha_R} R(t) = F_5(t, R), \\ {}^C D_{0+}^{\alpha_D} D(t) = F_6(t, D), \\ {}^C D_{0+}^{\alpha_W} W(t) = F_7(t, W), \end{cases} \quad (4)$$

where the function F_i , $1 \leq i \leq 7$, are the derivative functions on right side of system 1.

Thus, our approach unfolds in two steps. Initially, we establish positive values for the initial conditions. Subsequently, we apply the fractional order integral operator, which reconstitutes the system's equations as follows:

$$\begin{cases} S(t) - S(0) = I_{0+}^{\alpha_S} \left(\Lambda^{\alpha_S} - \frac{\beta_1^{\alpha_S} S(t)W(t)}{1+\phi_1 W(t)} - \frac{\beta_2^{\alpha_S} S(t)(I_A(t)+I_S(t))}{1+\phi_2(I_A(t)+I_S(t))} + \psi^{\alpha_S} E(t) - \mu^{\alpha_S} S(t) \right), \\ E(t) - E(0) = I_{0+}^{\alpha_E} \left(\frac{\beta_1^{\alpha_E} S(t)W(t)}{1+\phi_1 W(t)} + \frac{\beta_2^{\alpha_E} S(t)(I_A(t)+I_S(t))}{1+\phi_2(I_A(t)+I_S(t))} - \psi^{\alpha_E} E(t) - \mu^{\alpha_E} E(t) - \omega^{\alpha_E} E(t) \right), \\ I_A(t) - I_A(0) = I_{0+}^{\alpha_{I_A}} \left((1-\delta)\omega^{\alpha_{I_A}} E(t) - (\mu^{\alpha_{I_A}} + \sigma^{\alpha_{I_A}})I_A(t) - \gamma_A^{\alpha_{I_A}} I_A(t) \right), \\ I_S(t) - I_S(0) = I_{0+}^{\alpha_{I_S}} \left(\delta\omega^{\alpha_{I_S}} E(t) - (\mu^{\alpha_{I_S}} + \sigma^{\alpha_{I_S}})I_S(t) - \gamma_S^{\alpha_{I_S}} I_S(t) \right), \\ R(t) - R(0) = I_{0+}^{\alpha_R} \left(\gamma_S^{\alpha_R} I_S(t) + \gamma_A^{\alpha_R} I_A(t) - \mu^{\alpha_R} R(t) \right), \\ D(t) - D(0) = I_{0+}^{\alpha_D} \left(\sigma^{\alpha_D} (I_S(t) + I_A(t)) - \mu^{\alpha_D} D(t) \right), \\ W(t) - W(0) = I_{0+}^{\alpha_W} \left(\eta_A^{\alpha_W} I_A(t) + \eta_S^{\alpha_W} I_S(t) - \mu_P^{\alpha_W} W(t) \right). \end{cases} \quad (5)$$

Utilizing Equation 4, we derive the state variables expressed in terms of F_i as follows:

$$\begin{cases} S(t) = S(0) + \frac{1}{\Gamma(\alpha_S)} \int_0^t (t-\tau)^{\alpha_S-1} F_1(\tau, S(\tau)) d\tau, \\ E(t) = E(0) + \frac{1}{\Gamma(\alpha_E)} \int_0^t (t-\tau)^{\alpha_E-1} F_2(\tau, E(\tau)) d\tau, \\ I_A(t) = I_A(0) + \frac{1}{\Gamma(\alpha_{I_A})} \int_0^t (t-\tau)^{\alpha_{I_A}-1} F_3(\tau, I_A(\tau)) d\tau, \\ I_S(t) = I_S(0) + \frac{1}{\Gamma(\alpha_{I_S})} \int_0^t (t-\tau)^{\alpha_{I_S}-1} F_4(\tau, I_S(\tau)) d\tau, \\ R(t) = R(0) + \frac{1}{\Gamma(\alpha_R)} \int_0^t (t-\tau)^{\alpha_R-1} F_5(\tau, R(\tau)) d\tau, \\ D(t) = D(0) + \frac{1}{\Gamma(\alpha_D)} \int_0^t (t-\tau)^{\alpha_D-1} F_6(\tau, D(\tau)) d\tau, \\ W(t) = W(0) + \frac{1}{\Gamma(\alpha_W)} \int_0^t (t-\tau)^{\alpha_W-1} F_7(\tau, W(\tau)) d\tau. \end{cases} \quad (6)$$

Therefore, by applying the Picard iteration to Equation (6), we obtain the subsequent equations:

$$\begin{cases} S_{n+1}(t) = S(0) + \frac{1}{\Gamma(\alpha_S)} \int_0^t (t-\tau)^{\alpha_S-1} F_1(\tau, S(\tau)) d\tau, \\ E_{n+1}(t) = E(0) + \frac{1}{\Gamma(\alpha_E)} \int_0^t (t-\tau)^{\alpha_E-1} F_2(\tau, E(\tau)) d\tau, \\ I_{A_{n+1}}(t) = I_A(0) + \frac{1}{\Gamma(\alpha_{I_A})} \int_0^t (t-\tau)^{\alpha_{I_A}-1} F_3(\tau, I_A(\tau)) d\tau, \\ I_{S_{n+1}}(t) = I_S(0) + \frac{1}{\Gamma(\alpha_{I_S})} \int_0^t (t-\tau)^{\alpha_{I_S}-1} F_4(\tau, I_S(\tau)) d\tau, \\ R_{n+1}(t) = R(0) + \frac{1}{\Gamma(\alpha_R)} \int_0^t (t-\tau)^{\alpha_R-1} F_5(\tau, R(\tau)) d\tau, \\ D_{n+1}(t) = D(0) + \frac{1}{\Gamma(\alpha_D)} \int_0^t (t-\tau)^{\alpha_D-1} F_6(\tau, D(\tau)) d\tau, \\ W_{n+1}(t) = W(0) + \frac{1}{\Gamma(\alpha_W)} \int_0^t (t-\tau)^{\alpha_W-1} F_7(\tau, W(\tau)) d\tau. \end{cases} \quad (7)$$

To introduce the result, define $\mathbf{X}(t) = (S(t), E(t), I_A(t), I_S(t), R(t), D(t), W(t))^T$ as the state vector and

$\mathbf{F}(t, \mathbf{X}(t)) = (F_1(t, S(t)), F_2(t, E(t)), F_3(t, I_A(t)), F_4(t, I_S(t)), F_5(t, R(t)), F_6(t, D(t)), F_7(t, W(t)))^T$ as the vector of functions describing the system's dynamics. Furthermore, let $\mathbb{R}_+^7 = \{\mathbf{X} \in \mathbb{R}^7 : \mathbf{X} \geq 0\}$ representing the space of feasible states.

Lemma 1. *Let $f(t)$ be a function such that $f(t) \in C([0, T])$ and its Caputo fractional derivative ${}^C D_{0+}^\alpha f(t) \in C([0, T])$, with $0 < \alpha \leq 1$. Then, the following relation holds:*

$$f(t) = f(0) + \frac{1}{\Gamma(\alpha)} {}^C D_{0+}^\alpha f(\xi) (t-0)^\alpha, \quad (8)$$

where $0 \leq \xi \leq t$ for all $t \in (0, T]$. This relation represents the fractional generalization of the Mean Value Theorem, as established in [29].

Lemma 2. *Assuming the existence of a solution for system (1), said solution will maintain non-negativity provided that the initial conditions are also non-negative.*

Proof. To establish the result, we initially note the validity of the following conditions:

$$\begin{cases} {}^C D_{0+}^{\alpha_S} S(t)|_{S=0} = \Lambda^{\alpha_S} + \psi^{\alpha_S} E(t) \geq 0, \\ {}^C D_{0+}^{\alpha_E} E(t)|_{E=0} = \frac{\beta_1^{\alpha_E} S(t)W(t)}{1+\phi_1 W(t)} + \frac{\beta_2^{\alpha_E} S(t)(I_A(t)+I_S(t))}{1+\phi_2(t)(I_A(t)+I_S(t))} \geq 0, \\ {}^C D_{0+}^{\alpha_{I_A}} I_A(t)|_{I_A=0} = (1-\delta)\omega^{\alpha_{I_A}} E(t) \geq 0, \\ {}^C D_{0+}^{\alpha_{I_S}} I_S(t)|_{I_S=0} = \delta\omega^{\alpha_{I_S}} E(t) \geq 0, \\ {}^C D_{0+}^{\alpha_R} R(t)|_{R=0} = \gamma_S^{\alpha_R} I_S(t) + \gamma_A^{\alpha_R} I_A(t) \geq 0, \\ {}^C D_{0+}^{\alpha_D} D(t)|_{D=0} = \sigma^{\alpha_D} (I_S(t) + I_A(t)) \geq 0, \\ {}^C D_{0+}^{\alpha_W} W(t)|_{W=0} = \eta_A^{\alpha_W} I_A(t) + \eta_S^{\alpha_W} I_S(t) \geq 0, \end{cases} \quad (9)$$

for all $t \in [0, T]$. Given these conditions and referencing Lemma 1, it follows that the solution vector $\mathbf{X}(t) = (S(t), E(t), I_A(t), I_S(t), R(t), D(t), W(t))^\top$ of system (1) is contained within \mathbb{R}_+^7 . This observation conclusively verifies the non-negativity of the solution, thereby completing the proof. \square

Now, we endeavor to present and validate a pivotal outcome of our study. This outcome lays the foundational groundwork for establishing the existence and uniqueness of solutions for the system outlined in Equation (1), details of which will be elaborated upon subsequently.

Lemma 3. *The function $\mathbf{F}(t, \mathbf{X}(t))$ fulfills the Lipschitz conditions, specifically:*

$$\|\mathbf{F}(t, \mathbf{X}(t)) - \mathbf{F}(t, \mathbf{X}^*(t))\| \leq \Sigma \|\mathbf{X}(t) - \mathbf{X}^*(t)\|, \quad (10)$$

where

$$\begin{aligned} \Sigma = \max\{ & \left| \frac{\beta_1^{\alpha_S}}{\phi_1} + \frac{\beta_2^{\alpha_S}}{\phi_2} + \mu^{\alpha_S} \right|, |\psi^{\alpha_E} + \mu^{\alpha_E} + \omega^{\alpha_E}|, |\mu^{\alpha_{I_A}} + \sigma^{\alpha_{I_A}} + \gamma_A^{\alpha_{I_A}}|, \\ & |\mu^{\alpha_{I_S}} + \sigma^{\alpha_{I_S}} + \gamma_S^{\alpha_{I_S}}|, |\mu^{\alpha_R}|, |\mu^{\alpha_D}|, |\mu_p^{\alpha_W}| \}. \end{aligned} \quad (11)$$

Proof. Summarising that $S(t)$ and $S^*(t)$ are couple functions yields the following equality:

$$\|F_1(t, S(t)) - F_1(t, S^*(t))\| = \left\| \left(\frac{\beta_1^{\alpha_S} W(t)}{1 + \phi_1 W(t)} + \frac{\beta_2^{\alpha_S} (I_A(t) + I_S(t))}{1 + \phi_2 (I_A(t) + I_S(t))} + \mu^{\alpha_S} \right) (S(t) - S^*(t)) \right\|. \quad (12)$$

By defining

$$\Sigma_1 = \left| \frac{\beta_1^{\alpha_S}}{\phi_1} + \frac{\beta_2^{\alpha_S}}{\phi_2} + \mu^{\alpha_S} \right|, \quad (13)$$

we can infer the inequality:

$$\|F_1(t, S(t)) - F_1(t, S^*(t))\| \leq \Sigma_1 \|(S(t) - S^*(t))\|. \quad (14)$$

Proceeding similarly for the other functions yields:

$$\begin{aligned} \|F_2(t, E(t)) - F_2(t, E^*(t))\| &\leq \Sigma_2 \|(E(t) - E^*(t))\| \\ \|F_3(t, I_A(t)) - F_3(t, I_A^*(t))\| &\leq \Sigma_3 \|(I_A(t) - I_A^*(t))\| \\ \|F_4(t, I_S(t)) - F_4(t, I_S^*(t))\| &\leq \Sigma_4 \|(I_S(t) - I_S^*(t))\| \\ \|F_5(t, R(t)) - F_5(t, R^*(t))\| &\leq \Sigma_5 \|(R(t) - R^*(t))\| \\ \|F_6(t, D(t)) - F_6(t, D^*(t))\| &\leq \Sigma_6 \|(D(t) - D^*(t))\| \\ \|F_7(t, W(t)) - F_7(t, W^*(t))\| &\leq \Sigma_7 \|(W(t) - W^*(t))\|, \end{aligned} \quad (15)$$

with the Σ values specified as:

$$\Sigma_2 = |\psi^{\alpha_E} + \mu^{\alpha_E} + \omega^{\alpha_E}|,$$

$$\begin{aligned}
\Sigma_3 &= |\mu^{\alpha_{IA}} + \sigma^{\alpha_{IA}} + \gamma_A^{\alpha_{IA}}|, \\
\Sigma_4 &= |\mu^{\alpha_{IS}} + \sigma^{\alpha_{IS}} + \gamma_S^{\alpha_{IS}}|, \\
\Sigma_5 &= |\mu^{\alpha_R}|, \\
\Sigma_6 &= |\mu^{\alpha_D}|, \\
\Sigma_7 &= |\mu_p^{\alpha_W}|.
\end{aligned} \tag{16}$$

This analysis, from Equations (14) to (16), demonstrates that all seven functions, F_i , meet the Lipschitz condition, validating their properties for the system (1). \square

Theorem 1. *Given the conditions of Lemma 3, if the inequality*

$$\Sigma \max_i \frac{T^{\alpha_i}}{\Gamma(\alpha_i + 1)} < 1, \quad i = S, E, IA, IS, R, D, W, \tag{17}$$

is satisfied, then the system (1) admits a unique, positive solution.

Proof. The solution to system (1) can be expressed in the form:

$$\mathbf{X}(t) = P(\mathbf{X}(t)), \tag{18}$$

where $P : C([0, T], \mathbb{R}^7) \rightarrow C([0, T], \mathbb{R}^7)$ denotes the Picard operator. This operator is defined as follows:

$$\begin{aligned}
P(\mathbf{X}(t)) = \mathbf{X}(0) + \int_0^t \text{diag} \left(\frac{(t-\tau)^{\alpha_S-1}}{\Gamma(\alpha_S)}, \frac{(t-\tau)^{\alpha_E-1}}{\Gamma(\alpha_E)}, \frac{(t-\tau)^{\alpha_{IA}-1}}{\Gamma(\alpha_{IA})}, \frac{(t-\tau)^{\alpha_{IS}-1}}{\Gamma(\alpha_{IS})}, \right. \\
\left. \frac{(t-\tau)^{\alpha_R-1}}{\Gamma(\alpha_R)}, \frac{(t-\tau)^{\alpha_D-1}}{\Gamma(\alpha_D)}, \frac{(t-\tau)^{\alpha_W-1}}{\Gamma(\alpha_W)} \right) \mathbf{F}(\tau, \mathbf{X}(\tau)) d\tau.
\end{aligned} \tag{19}$$

Simultaneously, we encounter the series of inequalities below:

$$\begin{aligned}
\|P(\mathbf{X}(t)) - P(\mathbf{X}^*(t))\| &= \left\| \int_0^t \text{diag} \left(\frac{(t-\tau)^{\alpha_S-1}}{\Gamma(\alpha_S)}, \frac{(t-\tau)^{\alpha_E-1}}{\Gamma(\alpha_E)}, \right. \right. \\
&\quad \left. \frac{(t-\tau)^{\alpha_{IA}-1}}{\Gamma(\alpha_{IA})}, \frac{(t-\tau)^{\alpha_{IS}-1}}{\Gamma(\alpha_{IS})}, \frac{(t-\tau)^{\alpha_R-1}}{\Gamma(\alpha_R)}, \frac{(t-\tau)^{\alpha_D-1}}{\Gamma(\alpha_D)}, \frac{(t-\tau)^{\alpha_W-1}}{\Gamma(\alpha_W)} \right) \\
&\quad \times (\mathbf{F}(\tau, \mathbf{X}(\tau)) - \mathbf{F}(\tau, \mathbf{X}^*(\tau))) d\tau \Big\| \\
&\leq \left\| \int_0^t \text{diag} \left(\frac{(t-\tau)^{\alpha_S-1}}{\Gamma(\alpha_S)}, \frac{(t-\tau)^{\alpha_E-1}}{\Gamma(\alpha_E)}, \right. \right. \\
&\quad \left. \frac{(t-\tau)^{\alpha_{IA}-1}}{\Gamma(\alpha_{IA})}, \frac{(t-\tau)^{\alpha_{IS}-1}}{\Gamma(\alpha_{IS})}, \frac{(t-\tau)^{\alpha_R-1}}{\Gamma(\alpha_R)}, \frac{(t-\tau)^{\alpha_D-1}}{\Gamma(\alpha_D)}, \frac{(t-\tau)^{\alpha_W-1}}{\Gamma(\alpha_W)} \right) d\tau \Big\| \\
&\quad \times \sup_{\tau \in [0, T]} \|\mathbf{F}(\tau, \mathbf{X}(\tau)) - \mathbf{F}(\tau, \mathbf{X}^*(\tau))\| \\
&\leq \max_{i=S, E, IA, IS, R, D, W} \int_0^t \frac{(t-\tau)^{\alpha_i-1}}{\Gamma(\alpha_i)} d\tau \sup_{\tau \in [0, T]} \|\mathbf{F}(\tau, \mathbf{X}(\tau)) - \mathbf{F}(\tau, \mathbf{X}^*(\tau))\| \\
&\leq \Sigma \max_{i=S, E, IA, IS, R, D, W} \frac{T^{\alpha_i}}{\Gamma(\alpha_i + 1)} \sup_{\tau \in [0, T]} \|\mathbf{X}(\tau) - \mathbf{X}^*(\tau)\|.
\end{aligned} \tag{20}$$

Given that $\Sigma \max_{i \in \{S, E, IA, IS, R, D, W\}} \frac{T^{\alpha_i}}{\Gamma(\alpha_i + 1)} < 1$ for $t \leq T$, the operator P is established as a contraction. Consequently, system (1) is guaranteed to have a unique solution, thereby completing the proof. \square

3.3. Boundedness of the Solution

This section demonstrates the positive invariance and boundedness of the solutions within a biologically meaningful region for the model system (1).

Theorem 2. *Let Ω be the closed set defined by*

$$\Omega = \left\{ \mathbf{X} \in \mathbb{R}_+^7 : 0 \leq N(t) \leq \frac{\Lambda}{\mu}, 0 \leq W \leq \frac{\Lambda(\eta_A + \eta_S)}{\mu\mu_P} \right\}, \quad (21)$$

where $N(t) = S(t) + E(t) + I_A(t) + I_S(t) + R(t) + D(t)$ represents the total population at time t , excluding the environmental pathogen W . Then, Ω is positively invariant under the dynamics of the system (1) with commensurate orders for all $t > 0$, meaning that any solution starting within Ω remains in Ω for all future times.

Proof. To establish the theorem, we initially consider the case of integer order derivatives. Define the total population at time t as $N(t) = S(t) + E(t) + I_A(t) + I_S(t) + R(t) + D(t)$. According to system (1), the rate of change of $N(t)$ is given by

$$N'(t) = \Lambda - \mu N(t), \quad (22)$$

indicating a balance between birth and overall mortality rates. Multiplying both sides by $e^{\mu t}$ and integrating yields

$$e^{\mu t} N(t) = \frac{\Lambda}{\mu} e^{\mu t} + C, \quad (23)$$

where C is a constant determined by initial conditions, specifically $C = N_0 - \frac{\Lambda}{\mu}$ with $N_0 = N(0)$. This leads to

$$N(t) = N_0 e^{-\mu t} + \frac{\Lambda}{\mu} (1 - e^{-\mu t}), \quad (24)$$

and accordingly,

$$\limsup_{t \rightarrow \infty} N(t) = \frac{\Lambda}{\mu}. \quad (25)$$

For environmental pathogens, considering $I_A(t) + I_S(t) \leq N(t) \leq \frac{\Lambda}{\mu}$ and applying the last equation of (1), we deduce

$$W'(t) \leq (\eta_A + \eta_S) \frac{\Lambda}{\mu} - \mu_P W(t), \quad (26)$$

which implies

$$W(t) \leq W(0) e^{-\mu_P t} + \frac{(\eta_A + \eta_S) \Lambda}{\mu \mu_P} (1 - e^{-\mu_P t}), \quad (27)$$

ensuring

$$\limsup_{t \rightarrow \infty} W(t) \leq \frac{(\eta_A + \eta_S) \Lambda}{\mu \mu_P}. \quad (28)$$

Extending to commensurate fractional derivatives (when all orders are α) and utilizing a fractional comparison theorem, we find

$$N(t) = N_0 E_{\alpha,1}(-\mu t^\alpha) + \left(\frac{\Lambda}{\mu} \right)^\alpha E_{\alpha,\alpha+1}(-\mu t^\alpha), \quad (29)$$

where $E_{\alpha,\beta}$ is the asymptotic expansion of the Mittag-Leffler function. As t approaches infinity, this function's properties ensure $N(t)$ approaches $\left(\frac{\Lambda}{\mu} \right)^\alpha$, confirming that Ω is positively invariant.

Similarly, $\limsup_{t \rightarrow \infty} W(t) \leq \frac{(\eta_A + \eta_S) \Lambda^\alpha}{\mu^\alpha \mu_P^\alpha}$. \square

It is important to note that our model incorporates incommensurate orders of derivatives, which introduces additional complexity to the analysis of system dynamics. Specifically, the traditional approach of equating the sum of compartmental populations to the total population may not hold precisely due to the asynchronous nature of the derivative orders. This deviation poses challenges in directly applying conventional methods to ascertain the boundedness and stability of solutions.

However, recent advancements in the field have shed light on handling such complexities. Under certain conditions, the exponential boundedness of solutions for systems with incommensurate fractional derivatives has been demonstrated [30]. This suggests that, although the direct approach might falter, alternative strategies rooted in the latest mathematical frameworks can provide rigorous justification for the boundedness of solutions in our model. Such considerations are crucial for ensuring the robustness and biological fidelity of the model, especially when dealing with the behaviors exhibited by incommensurate order systems.

3.4. Basic reproduction number

The basic reproduction number is determined via the next-generation matrix method [31], applied to our model as specified in (1). This approach focuses on calculating the rate at which new infections emerge within the infectious compartments, denoted as $\mathcal{X} = (E, I_A, I_S, W)$, and is described as follows:

$$\mathcal{F}(\mathcal{X}) = \begin{pmatrix} \frac{\beta_1^{\alpha E} S(t)W(t)}{1+\phi_1 W(t)} + \frac{\beta_2^{\alpha E} S(t)(I_A(t)+I_S(t))}{1+\phi_2(I_A(t)+I_S(t))} \\ 0 \\ 0 \\ 0 \end{pmatrix},$$

and the rate of other transitions involving shedding compartment is obtained as follows

$$\mathcal{V}(\mathcal{X}) = \begin{pmatrix} (\psi^{\alpha E} + \mu^{\alpha E} + \omega^{\alpha E})E \\ (\mu^{\alpha I_A} + \sigma^{\alpha I_A} + \gamma_A^{\alpha I_A})I_A - (1-\delta)\omega^{\alpha I_A}E \\ (\mu^{\alpha I_S} + \sigma^{\alpha I_S} + \gamma_S^{\alpha I_S})I_S - \delta\omega^{\alpha I_S}E \\ \mu_P^{\alpha W}W - \eta_A^{\alpha W}I_A - \eta_S^{\alpha W}I_S. \end{pmatrix}.$$

We identify a discrepancy in the original model [10] concerning the calculation of the basic reproduction number, R_0 . Specifically, the definitions of \mathcal{F} and \mathcal{V} in their work do not align with standard practices. To address this, we redefine $-\eta_A^{\alpha W}I_A - \eta_S^{\alpha W}I_S$ accurately as a factor in the transition of new infections, rather than as a contributor to the generation of new infections. Following this correction, the Jacobian matrices for \mathcal{F} and \mathcal{V} at the disease-free equilibrium (DFE) point, $\mathfrak{E}_0 = \left(\left(\frac{\Lambda}{\mu} \right)^{\alpha_S}, 0, 0, 0, 0, 0, 0 \right)$, are derived as follows:

$$J_{\mathcal{F}} = \begin{bmatrix} 0 & \beta_2^{\alpha E} \left(\frac{\Lambda}{\mu} \right)^{\alpha_S} & \beta_2^{\alpha E} \left(\frac{\Lambda}{\mu} \right)^{\alpha_S} & \beta_1^{\alpha E} \left(\frac{\Lambda}{\mu} \right)^{\alpha_S} \\ 0 & 0 & 0 & 0 \\ 0 & 0 & 0 & 0 \\ 0 & 0 & 0 & 0 \end{bmatrix} \quad \text{and}$$

$$J_{\mathcal{V}} = \begin{bmatrix} \psi^{\alpha E} + \mu^{\alpha E} + \omega^{\alpha E} & 0 & 0 & 0 \\ -(1-\delta)\omega^{\alpha I_A} & \mu^{\alpha I_A} + \sigma^{\alpha I_A} + \gamma_A^{\alpha I_A} & 0 & 0 \\ -\delta\omega^{\alpha I_S} & 0 & \mu^{\alpha I_S} + \sigma^{\alpha I_S} + \gamma_S^{\alpha I_S} & 0 \\ 0 & -\eta_A^{\alpha W} & -\eta_S^{\alpha W} & \mu_P^{\alpha W} \end{bmatrix}.$$

Finally, the basic reproduction number R_0 is obtained as the spectral radius of generation matrix $J_{\mathcal{F}} \cdot J_{\mathcal{V}}^{-1}$, that is precisely

$$R_0 = (\Lambda/\mu)^{\alpha_S} \left(\beta_2^{\alpha E} \left(\frac{\delta\omega^{\alpha I_S}}{\varpi_{is}\varpi_e} + \frac{(1-\delta)\omega^{\alpha I_A}}{\varpi_{ia}\varpi_e} \right) + \beta_1^{\alpha E} \left(\frac{\eta_S^{\alpha W}\delta\omega^{\alpha I_S}}{\mu_P^{\alpha W}\varpi_e\varpi_{is}} + \frac{\eta_A^{\alpha W}(1-\delta)\omega^{\alpha I_A}}{\mu_P^{\alpha W}\varpi_e\varpi_{ia}} \right) \right), \quad (30)$$

where

$$\varpi_e = \psi^{\alpha E} + \mu^{\alpha E} + \omega^{\alpha E}, \quad \varpi_{ia} = \mu^{\alpha I_A} + \sigma^{\alpha I_A} + \gamma_A^{\alpha I_A}, \quad \varpi_{is} = \mu^{\alpha I_S} + \sigma^{\alpha I_S} + \gamma_S^{\alpha I_S}.$$

3.5. Local stability analysis

In this section, we focus on establishing the local stability of the disease-free equilibrium point, denoted as \mathfrak{E}_0 , for the model described in Equation (1). This is achieved by analyzing the eigenvalues derived from the linearization matrix, specifically the system's Jacobian $J(\mathfrak{E}_0)$.

Theorem 3. ([32]) *Assuming the conditions $0 < \alpha_i \leq 1$ for each $i = S, E, I_A, I_S, R, D, W$, let M represent lowest common multiple of r_i and q_i , where $\alpha_i = \frac{r_i}{q_i}$ with $r_i, q_i \in \mathbb{N}$, such that $\gcd(r_i, q_i) = 1, \forall i = S, E, I_A, I_S, R, D, W$. If every root λ of the equation*

$$\det(\text{diag}(\lambda^{r_1}, \lambda^{r_2}, \lambda^{r_3}, \lambda^{r_4}, \lambda^{r_5}, \lambda^{r_6}, \lambda^{r_7}) - J(\mathfrak{E}_0)) = 0, \quad (31)$$

fulfills the condition $|\arg(\lambda)| > \frac{\pi}{2M}$, then the system's equilibrium is locally asymptotically stable.

Theorem 4. *If $\alpha_E = \alpha_{I_A} = \alpha_{I_S} = \alpha_W = \alpha$ holds, the disease-free equilibrium point \mathfrak{E}_0 of model (1) is locally asymptotically stable if the eigenvalues of $J(\mathfrak{E}_0)$ meet the criteria set forth in Theorem 3.*

Proof. The Jacobian of Equation (1), evaluated at the disease-free equilibrium \mathfrak{E}_0 is

$$J(\mathfrak{E}_0) = \begin{pmatrix} -\mu^{\alpha_S} & \psi^{\alpha_S} & \mathcal{A} & \mathcal{A} & 0 & 0 & \mathcal{B} \\ 0 & \mathcal{E} & \mathcal{C} & \mathcal{C} & 0 & 0 & \mathcal{D} \\ 0 & (1-\delta)\omega^{\alpha_{I_A}} & \mathcal{F} & 0 & 0 & 0 & 0 \\ 0 & \delta\omega^{\alpha_{I_S}} & 0 & \mathcal{G} & 0 & 0 & 0 \\ 0 & 0 & \gamma_A^{\alpha_R} & \gamma_S^{\alpha_R} & -\mu^{\alpha_R} & 0 & 0 \\ 0 & 0 & \sigma^{\alpha_D} & \sigma^{\alpha_D} & 0 & -\mu^{\alpha_D} & 0 \\ 0 & 0 & \eta_A^{\alpha_W} & \eta_S^{\alpha_W} & 0 & 0 & -\mu_P^{\alpha_W} \end{pmatrix},$$

where $\mathcal{A} = -\frac{\beta_2^{\alpha_S} \Lambda^{\alpha_S}}{\mu^{\alpha_S}}$, $\mathcal{B} = -\frac{\beta_1^{\alpha_S} \Lambda^{\alpha_S}}{\mu^{\alpha_S}}$, $\mathcal{C} = \frac{\beta_2^{\alpha_E} \Lambda^{\alpha_S}}{\mu^{\alpha_S}}$, $\mathcal{D} = \frac{\beta_1^{\alpha_E} \Lambda^{\alpha_S}}{\mu^{\alpha_S}}$, $\mathcal{E} = -(\psi^{\alpha_E} + \mu^{\alpha_E} + \omega^{\alpha_E})$, $\mathcal{F} = -(\mu^{\alpha_{I_A}} + \sigma^{\alpha_{I_A}} + \gamma_A^{\alpha_{I_A}})$, $\mathcal{G} = -(\mu^{\alpha_{I_S}} + \sigma^{\alpha_{I_S}} + \gamma_S^{\alpha_{I_S}})$.

The characteristic equation derived from $J(\mathfrak{E}_0)$ simplifies to

$$\det(\text{diag}(\lambda^{M\alpha_S}, \lambda^{M\alpha_E}, \lambda^{M\alpha_{I_A}}, \lambda^{M\alpha_{I_S}}, \lambda^{M\alpha_R}, \lambda^{M\alpha_D}, \lambda^{M\alpha_W}) - J(\mathfrak{E}_0)) = 0$$

Given the assumption that $\alpha_E = \alpha_{I_A} = \alpha_{I_S} = \alpha_W = \alpha$ it follows that:

$$(\lambda^{M\alpha_S} + \mu^{\alpha_S})(\lambda^{M\alpha_R} + \mu^{\alpha_R})(\lambda^{M\alpha_W} + \mu^{\alpha_W})(\lambda^{4M\alpha} + \mathcal{H}_1\lambda^{3M\alpha} + \mathcal{H}_2\lambda^{2M\alpha} + \mathcal{H}_3\lambda^{M\alpha} + \mathcal{H}_4) = 0, \quad (32)$$

where

$$\begin{aligned} \mathcal{H}_1 &= \mathcal{E} + \mathcal{F} + \mathcal{G} + \mu_P^\alpha \\ \mathcal{H}_2 &= \mathcal{E}\mathcal{F} + \mathcal{E}\mathcal{G} + \mathcal{F}\mathcal{G} + \mu_P^\alpha(\mathcal{E} + \mathcal{F} + \mathcal{G}) - \mathcal{C}\omega^\alpha \\ \mathcal{H}_3 &= \mathcal{E}\mathcal{F}\mathcal{G} - \omega^\alpha(\mathcal{C}(\mathcal{G} - \mu_P^\alpha + (\mathcal{G} - \mathcal{F})\delta) + \mathcal{D}\eta_S^\alpha) + \mathcal{D}\eta_A^\alpha\omega^\alpha(1-\delta) + \mu_P^\alpha(\mathcal{E}\mathcal{F} + \mathcal{E}\mathcal{G} + \mathcal{F}\mathcal{G}) \\ \mathcal{H}_4 &= \mathcal{E}\mathcal{F}\mathcal{G}\mu_P^\alpha + \omega^\alpha(\mathcal{G}(1-\delta)(\mathcal{D}\eta_A^\alpha + \mathcal{C}\mu_P^\alpha) + \mathcal{F}\delta(\mathcal{D}\eta_S^\alpha - \mathcal{C}\mu_P^\alpha)). \end{aligned}$$

From the initial terms of Equation (32), specifically $(\lambda^{M\alpha_S} + \mu^{\alpha_S}) = 0$, we directly obtain:

$$\arg(\lambda_{1,k}) = \frac{\pi}{M\alpha_S} + 2\frac{k\pi}{M\alpha_S}.$$

This leads us to conclude:

$$|\arg(\lambda_{1,k})| > \frac{\pi}{2M}, \quad k = 0, 1, \dots, M\alpha_S - 1.$$

Likewise, examining the second and third terms of Equation (32), it follows that:

$$\begin{aligned} |\arg(\lambda_{2,k})| &> \frac{\pi}{2M}, \quad k = 0, 1, \dots, M\alpha_R - 1, \\ |\arg(\lambda_{3,k})| &> \frac{\pi}{2M}, \quad k = 0, 1, \dots, M\alpha_W - 1. \end{aligned}$$

The remaining eigenvalues can be determined as the solutions to the equation

$$\mathfrak{P}(\lambda^{M\alpha}) = (\lambda^{M\alpha})^4 + \mathcal{H}_1(\lambda^{M\alpha})^3 + \mathcal{H}_2(\lambda^{M\alpha})^2 + \mathcal{H}_3(\lambda^{M\alpha}) + \mathcal{H}_4 = 0.$$

Based on Theorem 3, it is required that $|\arg(\lambda)| > \frac{\pi}{2M}$. Given that $M\alpha$ is a positive integer, this implies $M\alpha|\arg(\lambda)| > \frac{\alpha\pi}{2}$, which in turn implies $|\arg(\lambda^{M\alpha})| > \frac{\alpha\pi}{2}$. This satisfies the Routh-Hurwitz conditions, as elucidated in [33, 34], which are necessary and sufficient for the stability of the roots of the polynomial equation. We now proceed to define the discriminant of $\mathfrak{P}(\lambda)$ as follows:

$$\mathfrak{D}(\mathfrak{P}) = \begin{bmatrix} 1 & \mathcal{H}_1 & \mathcal{H}_2 & \mathcal{H}_3 & \mathcal{H}_4 & 0 & 0 \\ 0 & 1 & \mathcal{H}_1 & \mathcal{H}_2 & \mathcal{H}_3 & \mathcal{H}_4 & 0 \\ 0 & 0 & 1 & \mathcal{H}_1 & \mathcal{H}_2 & \mathcal{H}_3 & \mathcal{H}_4 \\ 4 & 3\mathcal{H}_1 & 2\mathcal{H}_2 & \mathcal{H}_3 & 0 & 0 & 0 \\ 0 & 4 & 3\mathcal{H}_1 & 2\mathcal{H}_2 & \mathcal{H}_3 & 0 & 0 \\ 0 & 0 & 4 & 3\mathcal{H}_1 & 2\mathcal{H}_2 & \mathcal{H}_3 & 0 \\ 0 & 0 & 0 & 4 & 3\mathcal{H}_1 & 2\mathcal{H}_2 & \mathcal{H}_3 \end{bmatrix}.$$

Leveraging insights from [33, 34], the stability criteria for the equilibrium point \mathfrak{E}_0 are as follows:

1. If

$$\Delta_1 = \mathcal{H}_1, \quad \Delta_2 = \begin{vmatrix} \mathcal{H}_1 & 1 \\ \mathcal{H}_3 & \mathcal{H}_2 \end{vmatrix}, \quad \Delta_3 = \begin{vmatrix} \mathcal{H}_1 & 1 & 0 \\ \mathcal{H}_3 & \mathcal{H}_2 & \mathcal{H}_1 \\ 0 & \mathcal{H}_4 & \mathcal{H}_3 \end{vmatrix},$$

then in the scenario where $\alpha = 1$, the necessary and sufficient condition for the equilibrium point \mathfrak{E}_0 to be locally asymptotically stable are

$$\Delta_1 > 0, \Delta_2 > 0, \Delta_3 = 0, \mathcal{H}_4 > 0,$$

and the above conditions are sufficient for \mathfrak{E}_0 to be locally asymptotically stable for all $\alpha \in [0, 1)$.

2. If $\mathfrak{D}(\mathfrak{P}) > 0, \mathcal{H}_1 > 0, \mathcal{H}_2 < 0$ and $\alpha > \frac{2}{3}$, then the equilibrium point \mathfrak{E}_0 is unstable.
3. If $\mathfrak{D}(\mathfrak{P}) < 0, \mathcal{H}_1 > 0, \mathcal{H}_2 > 0, \mathcal{H}_3 > 0, \mathcal{H}_4 > 0$ and $\alpha < \frac{1}{3}$, then the equilibrium point \mathfrak{E}_0 is locally asymptotically stable.
Furthermore, if $\mathfrak{D}(\mathfrak{P}) < 0, \mathcal{H}_1 < 0, \mathcal{H}_2 > 0, \mathcal{H}_3 < 0, \mathcal{H}_4 > 0$, then the equilibrium point \mathfrak{E}_0 is unstable.
4. If $\mathfrak{D}(\mathfrak{P}) < 0, \mathcal{H}_1 > 0, \mathcal{H}_2 > 0, \mathcal{H}_3 > 0, \mathcal{H}_4 > 0$ and $\frac{\mathcal{H}_1\mathcal{H}_4}{\mathcal{H}_2\mathcal{H}_3} + \frac{\mathcal{H}_3}{\mathcal{H}_1} > \frac{\mathcal{H}_4}{\mathcal{H}_1}$, then the equilibrium point \mathfrak{E}_0 is locally asymptotically stable, for all $\alpha \in (0, 1)$.
5. $\mathcal{H}_4 > 0$ is the necessary condition for the equilibrium point \mathfrak{E}_0 to be locally asymptotically stable.

□

3.6. Global stability analysis

Here, we investigate the global stability of the steady state when the disease is dying out in the population.

Theorem 5. *The disease-free equilibrium point (\mathfrak{E}_0) of system (1) is globally asymptotically stable whenever $R_0 \leq 1$.*

Proof. Let us consider the following Lyapunov function:

$$V(t) = b_0E(t) + b_1I_A(t) + b_2I_S(t) + b_3W(t),$$

where b_1, b_1, b_2 , and b_3 are positive constant to be determined.

By linearity of the Caputo derivative, we have

$${}^C D_{0+}^\alpha V(t) = b_0 {}^C D_{0+}^\alpha E(t) + b_1 {}^C D_{0+}^\alpha I_A(t) + b_2 {}^C D_{0+}^\alpha I_S(t) + b_3 {}^C D_{0+}^\alpha W(t).$$

Next, by substituting expression of ${}^C D_{0+}^\alpha E(t)$, ${}^C D_{0+}^\alpha I_A(t)$, ${}^C D_{0+}^\alpha I_S(t)$ and ${}^C D_{0+}^\alpha W(t)$ from system model (1), we obtain

$$\begin{aligned} {}^C D_{0+}^\alpha V(t) &= b_0 \left(\frac{\beta_1^{\alpha E} S(t)W(t)}{1 + \phi_1 W(t)} + \frac{\beta_2^{\alpha E} S(t)(I_A(t) + I_S(t))}{1 + \phi_2 (I_A(t) + I_S(t))} - \psi^{\alpha E} E(t) - \mu^{\alpha E} E(t) - \omega^{\alpha E} E(t) \right) \\ &\quad + b_1 \left((1 - \delta)\omega^{\alpha I_A} E(t) - (\mu^{\alpha I_A} + \sigma^{\alpha I_A})I_A(t) - \gamma_A^{\alpha I_A} I_A(t) \right) \\ &\quad + b_2 \left(\delta\omega^{\alpha I_S} E(t) - (\mu^{\alpha I_S} + \sigma^{\alpha I_S})I_S(t) - \gamma_S^{\alpha I_S} I_S(t) \right) \\ &\quad + b_3 \left(\eta_A^{\alpha W} I_A(t) + \eta_S^{\alpha W} I_S(t) - \mu_P^{\alpha W} W(t) \right). \end{aligned}$$

Since, the inequality $S \leq (\frac{\Lambda}{\mu})^{\alpha S}$ holds, it follows that

$$\begin{aligned} {}^C D_{0+}^\alpha V(t) &\leq b_0 \left(\left(\frac{\Lambda}{\mu} \right)^{\alpha S} \left(\frac{\beta_1^{\alpha E} W(t)}{1 + \phi_1 W(t)} + \frac{\beta_2^{\alpha E} (I_A(t) + I_S(t))}{1 + \phi_2 (I_A(t) + I_S(t))} \right) - \psi^{\alpha E} E(t) - \mu^{\alpha E} E(t) - \omega^{\alpha E} E(t) \right) \\ &\quad + b_1 \left((1 - \delta)\omega^{\alpha I_A} E(t) - (\mu^{\alpha I_A} + \sigma^{\alpha I_A})I_A(t) - \gamma_A^{\alpha I_A} I_A(t) \right) \\ &\quad + b_2 \left(\delta\omega^{\alpha I_S} E(t) - (\mu^{\alpha I_S} + \sigma^{\alpha I_S})I_S(t) - \gamma_S^{\alpha I_S} I_S(t) \right) \\ &\quad + b_3 \left(\eta_A^{\alpha W} I_A(t) + \eta_S^{\alpha W} I_S(t) - \mu_P^{\alpha W} W(t) \right). \end{aligned}$$

Note that because parameters and state variables are positive, we have

$$\frac{1}{1 + \phi_1 W} \leq 1, \quad \text{and} \quad \frac{1}{1 + \phi_2 (I_A + I_S)} \leq 1.$$

It follows that

$$\begin{aligned} {}^C D_{0+}^\alpha V(t) &\leq b_0 \left(\left(\frac{\Lambda}{\mu} \right)^{\alpha S} (\beta_1^{\alpha E} W(t) + \beta_2^{\alpha E} (I_A(t) + I_S(t))) - \psi^{\alpha E} E(t) - \mu^{\alpha E} E(t) - \omega^{\alpha E} E(t) \right) \\ &\quad + b_1 \left((1 - \delta)\omega^{\alpha I_A} E(t) - (\mu^{\alpha I_A} + \sigma^{\alpha I_A})I_A(t) - \gamma_A^{\alpha I_A} I_A(t) \right) \\ &\quad + b_2 \left(\delta\omega^{\alpha I_S} E(t) - (\mu^{\alpha I_S} + \sigma^{\alpha I_S})I_S(t) - \gamma_S^{\alpha I_S} I_S(t) \right) \\ &\quad + b_3 \left(\eta_A^{\alpha W} I_A(t) + \eta_S^{\alpha W} I_S(t) - \mu_P^{\alpha W} W(t) \right). \end{aligned}$$

Rearranging and reducing lead to the following expression

$$\begin{aligned} {}^C D_{0+}^\alpha V(t) &\leq (b_2 \delta \omega^{\alpha I_S} - b_0 \varpi_e - b_1 \omega^{\alpha I_A} (\delta - 1)) E(t) \\ &\quad + (b_3 \eta_A^{\alpha W} - b_1 \varpi_{ia} + b_0 \beta_2^{\alpha E} \left(\frac{\Lambda}{\mu} \right)^{\alpha S}) I_A(t) \\ &\quad + (b_3 \eta_S^{\alpha W} - b_2 \varpi_{is} + b_0 \beta_2^{\alpha E} \left(\frac{\Lambda}{\mu} \right)^{\alpha S}) I_S(t) \\ &\quad + (b_0 \beta_1^{\alpha E} \left(\frac{\Lambda}{\mu} \right)^{\alpha S} - b_3 \mu_P^{\alpha W}) W(t), \end{aligned} \tag{33}$$

in which $\varpi_{is} = \gamma_S^{\alpha I_S} + \mu^{\alpha I_S} + \sigma^{\alpha I_S}$, $\varpi_{ia} = \gamma_A^{\alpha I_A} + \mu^{\alpha I_A} + \sigma^{\alpha I_A}$, and $\varpi_e = \mu^{\alpha E} + \omega^{\alpha E} + \psi^{\alpha E}$. Therefore, by choosing

$$\begin{aligned} b_0 &= \mu_P^{\alpha W} \varpi_{ia} \varpi_{is} \mu^{\alpha S}, \quad b_1 = \Lambda^{\alpha S} (\beta_1^{\alpha E} \eta_A^{\alpha W} + \beta_2^{\alpha E} \mu_P^{\alpha W}) \varpi_{is}, \\ b_2 &= \Lambda^{\alpha S} (\beta_1^{\alpha E} \eta_S^{\alpha W} + \beta_2^{\alpha E} \mu_P^{\alpha W}) \varpi_{ia} \quad b_3 = \Lambda^{\alpha S} \beta_1^{\alpha E} \varpi_{ia} \varpi_{is}, \end{aligned}$$

it easy to see that V is continuous and positive definite for all $E(t) > 0$, $I_A(t) > 0$, $I_S(t) > 0$ and $W(t) > 0$. As a consequence, we obtain that

$$b_3 \eta_A^{\alpha W} - b_1 \varpi_{is} + b_0 \beta_2^{\alpha E} \left(\frac{\Lambda}{\mu} \right)^{\alpha S} = 0, \quad b_3 \eta_S^{\alpha W} - b_2 \varpi_{ia} + b_0 \beta_2^{\alpha E} \left(\frac{\Lambda}{\mu} \right)^{\alpha S} = 0, \quad b_0 \beta_1^{\alpha E} \left(\frac{\Lambda}{\mu} \right)^{\alpha S} - b_3 \mu_P^{\alpha W} = 0,$$

$$\text{and } b_2\delta\omega^{\alpha I_S} - b_0\varpi_e - b_1\omega^{\alpha I_A}(\delta - 1) = \mu_P^{\alpha w} \varpi_{ia} \varpi_{is} \mu^{\alpha S} (R_0 - 1).$$

Hence, putting altogether in the inequality (33), we get

$${}^C D_{0+}^{\alpha} V(t) \leq \mu_P \varpi_{ia} \varpi_{is} \mu (R_0 - 1).$$

Finally, ${}^C D_{0+}^{\alpha} V(t) \leq 0$ if $R_0 \leq 1$. In addition, it is not hard to verify that the largest invariant set of $\{(S, E, I_A, I_S, R, D, W) \in \mathbb{R}^7 : {}^C D_{0+}^{\alpha} V(t) = 0\}$ is the singleton $\{\mathfrak{E}_0\}$. Hence, by LaSalle's invariance principle [35], we conclude that the disease-free equilibrium \mathfrak{E}_0 is globally asymptotically stable. \square

Our examination of global stability spans the entire spectrum of R_0 values, albeit within the scope of commensurate orders. Global stability of the commensurate fractional form of model (1) is confirmed through Ulam-Hyers stability [36], with recent COVID-19 model applications in [37].

To provide a foundation for the subsequent discussion, we introduce the inequality expressed as follows:

$$|{}^C D_{0+}^{\alpha} \mathbf{X}(t) - \mathbf{F}(t, \mathbf{X}(t))| \leq \epsilon, \quad t \in [0, T]. \quad (34)$$

We say a function $\bar{\mathbf{X}} \in \mathbb{R}_+^7$ is a solution of (34) if and only if there exists $h \in \mathbb{R}_+^7$ satisfying

1. $|h(t)| \leq \epsilon$
2. ${}^C D_{0+}^{\alpha} \bar{\mathbf{X}}(t) = \mathbf{F}(t, \bar{\mathbf{X}}(t)) + h(t), \quad t \in [0, T].$

Notably, by applying Equation (6) alongside property 2 mentioned above, straightforward simplification reveals that any function $\bar{\mathbf{X}} \in \mathbb{R}_+^7$ meeting the conditions of Equation (34) likewise fulfills the following associated integral inequality:

$$|\bar{\mathbf{X}}(t) - \bar{\mathbf{X}}(0) - \frac{1}{\Gamma(\alpha)} \int_0^t (t - \tau)^{\alpha-1} \mathbf{F}(\tau, \bar{\mathbf{X}}(\tau))| \leq \frac{T^{\alpha}}{\Gamma(\alpha + 1)} \epsilon. \quad (35)$$

Let $\mathfrak{F} = C([0, T]; \mathbb{R})$ denote the Banach space of all continuous functions from $[0, T]$ to \mathbb{R} equipped with the norm $\|\mathbf{X}\|_{\mathfrak{F}} = \sup_{t \in [0, T]} \{|\mathbf{X}|\}$, where $|\mathbf{X}| = |S(t)| + |E(t)| + |I_A(t)| + |I_S(t)| + |R(t)| + |D(t)| + |W(t)|$.

The fractional order model (1) achieves Ulam-Hyers stability if there are some $\Sigma > 0$ ensuring that, for any given ϵ , and for every solution $\bar{\mathbf{X}}$ meeting the conditions of (34), a corresponding solution \mathbf{X} to (4) can be found where

$$\|\bar{\mathbf{X}}(t) - \mathbf{X}(t)\|_{\mathfrak{F}} \leq \Sigma \epsilon, \quad t \in [0, T]. \quad (36)$$

Moreover, this model is deemed to be generalized Ulam-Hyers stable if a continuous function $\Sigma_F : \mathbb{R}_+ \rightarrow \mathbb{R}_+$ exists, satisfying $\Sigma_F(0) = 0$. This condition requires that, for any solution $\bar{\mathbf{X}}$ of (34), there must be a corresponding solution \mathbf{X} of (4) for which

$$\|\bar{\mathbf{X}}(t) - \mathbf{X}(t)\|_{\mathfrak{F}} \leq \Sigma_F \epsilon, \quad t \in [0, T]. \quad (37)$$

We proceed to detail the stability results for the fractional order model.

Theorem 6. *Assuming the conditions and conclusions of Lemma 3 and Theorem 1 are satisfied, i.e. $\Sigma \frac{T^{\alpha}}{\Gamma(\alpha+1)} < 1$, it follows that the model specified in (4) exhibits generalized Ulam-Hyers stability.*

Proof. Given that \mathbf{X} is a unique solution to (4) confirmed by Lemma 3 and Theorem 1, and $\bar{\mathbf{X}}$ meets the criteria of (34), reference to equations (6) and (35) leads us to conclude that for any

$\epsilon > 0$ and $t \in [0, T]$, the following relationship holds:

$$\begin{aligned}
\|\bar{\mathbf{X}} - \mathbf{X}\|_{\mathfrak{F}} &= \sup_{t \in [0, T]} |\bar{\mathbf{X}} - \mathbf{X}| \\
&= \sup_{t \in [0, T]} \left| \bar{\mathbf{X}} - \mathbf{X}_0 - \frac{1}{\Gamma(\alpha)} \int_0^t (t - \tau)^{\alpha-1} \mathbf{F}(t, \mathbf{X}(\tau)) d\tau \right| \\
&\leq \sup_{t \in [0, T]} \left| \bar{\mathbf{X}}(t) - \bar{\mathbf{X}}_0 - \frac{1}{\Gamma(\alpha)} \int_0^t (t - \tau)^{\alpha-1} \mathbf{F}(t, \bar{\mathbf{X}}(\tau)) d\tau \right| \\
&\quad + \sup_{t \in [0, T]} \frac{1}{\Gamma(\alpha)} \int_0^t (t - \tau)^{\alpha-1} |\mathbf{F}(t, \bar{\mathbf{X}}(\tau)) - \mathbf{F}(t, \mathbf{X}(\tau))| d\tau \\
&\leq \frac{\epsilon T^\alpha}{\Gamma(\alpha + 1)} + \frac{\Sigma}{\Gamma(\alpha)} \sup_{t \in [0, T]} \int_0^t (t - \tau)^{\alpha-1} |\bar{\mathbf{X}}(\tau) - \mathbf{X}(\tau)| d\tau \\
&\leq \frac{\epsilon T^\alpha}{\Gamma(\alpha + 1)} + \frac{\Sigma T^\alpha}{\Gamma(\alpha + 1)} \|\bar{\mathbf{X}}(\tau) - \mathbf{X}(\tau)\|_{\mathfrak{F}}.
\end{aligned} \tag{38}$$

From this, we derive that $\|\bar{\mathbf{X}} - \mathbf{X}\|_{\mathfrak{F}} \leq \Sigma_F \epsilon$, with Σ_F defined as $\frac{T^\alpha}{\Gamma(\alpha+1) - T^\alpha \Sigma}$. \square

4. Numerical results

In this section, we demonstrate the capability of Model (1) to simulate the dynamics of COVID-19 transmission. This includes consideration for environmental contamination by infected individuals. Additionally, we compare the basic reproduction number, R_0 , and its sensitivity across various scenarios and model configurations. The model is fine-tuned using data collected from South Africa, obtained from Johns Hopkins University's Center for Systems Science and Engineering (CSSE) [38].

South Africa confirmed its first case of COVID-19 in March 2020, prompting a National State of Disaster to be declared on March 15. A nationwide lockdown was then imposed on March 26. To better understand the spread of the disease in South Africa, our study focuses on simulating its propagation from the start of the lockdown measures until the end of the first peak of the epidemic, which occurred on September 22, 2020. In light of the United Nations documentation, as reported by the Department of Economic and Social Affairs, Population Division, World Population Prospects 2022, we incorporate a birth rate of $\Lambda = 19.995/1000$ (19.995 births per 1000 individuals) and a natural human death rate of $\mu = 9.468/1000$, while also assuming the initial conditions $I_S(0) = 17$, $R(0) = 0$, and $D(0) = 0$, based on the early phase of the epidemic.

We determine the remaining parameter values and initial conditions by fitting model (1) to the available data: daily new confirmed cases, recovered individuals, and deceased individuals. For parameters $\mu_p, \phi_1, \phi_2, \beta_1, \beta_2, \delta, \psi, \omega, \sigma, \gamma_S, \gamma_A, \eta_S, \eta_A$, we assume truncated normal distributions. These parameters must fall within a certain range of 0 to 1. The prior for the initial susceptible population, $S(0)$, is set to a truncated normal distribution with a wide range (1000 to 1500000) and large deviation, reflecting the variability in population sizes for different regions or countries. The initial conditions for exposed, $E(0)$, asymptomatic infectious, $I_A(0)$, and pathogen presence, $W(0)$, compartments are also set to truncated normal distributions. These distributions have ranges reflecting possible small initial values (0 to 300), based on the early phase of an epidemic when these compartments start to grow.

We optimize the order derivatives to examine the efficacy of fractional orders in the fitting process. We utilize the root mean square deviation (RMSD) as a measure of the model accuracy, where $\text{RMSD}(x, \hat{x}) = \sqrt{\frac{1}{n} \sum_{t=1}^n (x_t - \hat{x}_t)^2}$. Here, n denotes the number of data points, x denotes the estimated values, and \hat{x} denotes the actual values. Notably, considering biologically or clinically meaningful parameters plays a crucial role when fitting a model to data. For instance, previous research studies [39, 40] suggest that the parameters γ_S and γ_A should be confined to the range of (0,1). Given this point, we have chosen to display a set of fitted results, rather than solely

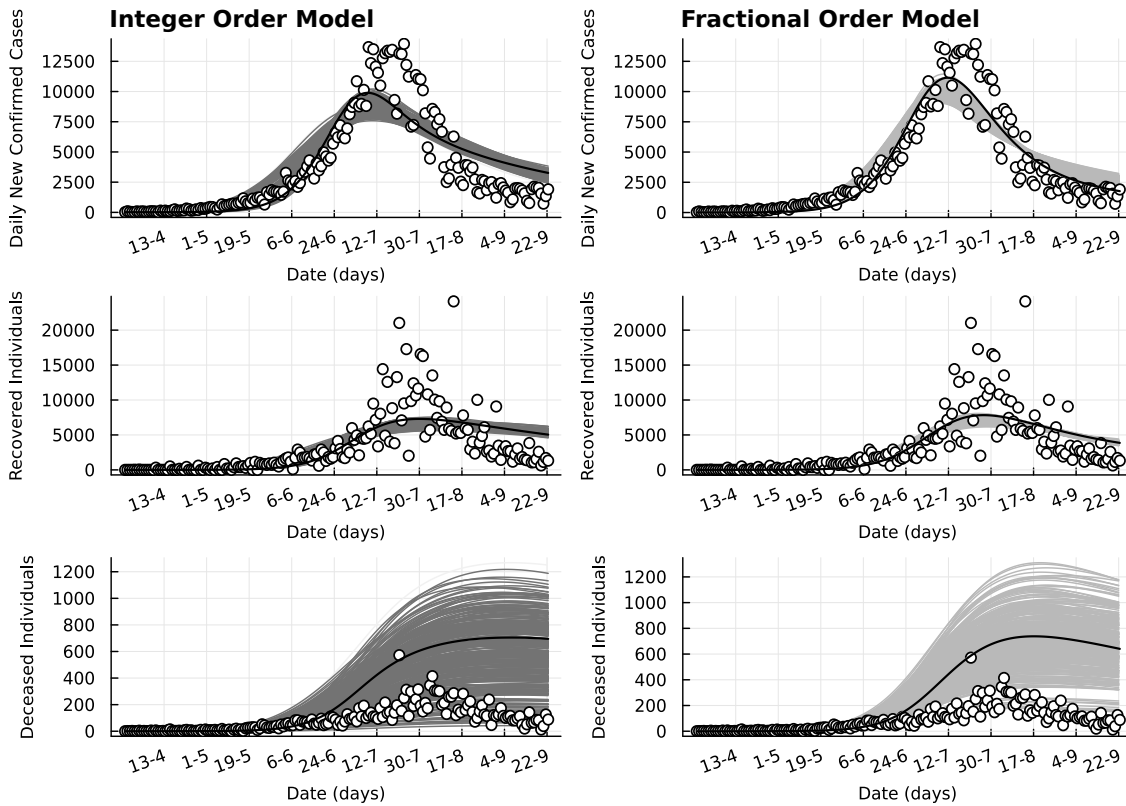


Figure 1: Model Accuracy Assessment: It demonstrates the accuracy of the model (1), with integer order derivatives (left panels) and fractional order derivatives (right panels), in fitting the daily new confirmed cases, recovered individuals, and deceased individuals, obtained from CSSE [38]. The circles represent the data points. The grey curves show the model's results with estimated parameter values and initial conditions, and the optimal fit across all three categories, evaluated via root mean square deviation (RMSD), is depicted with black curves.

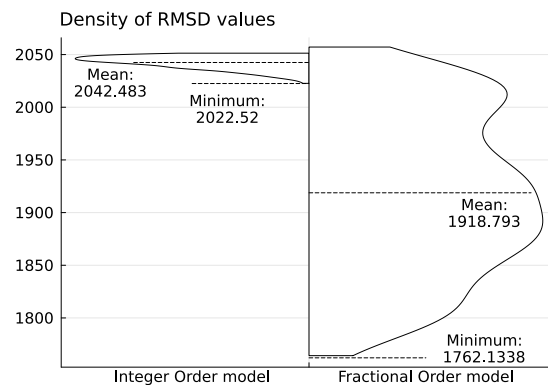


Figure 2: Comparative Error Score Distribution: It illustrates the distribution of root mean square deviation (RMSD) comparing real data with the fitted models using integer (left) and fractional (right) orders.

presenting the best fit, to demonstrate the overall efficiency of the model utilizing fractional calculus.

In Figure 1(left panels), the Bayesian inference method has been employed to provide initial estimates for both the parameter values and initial conditions, as the results depicted by the grey

curves and the black curve represents the best fit with an RMSD of 2022.52. In Figure 1(right panels), we have further optimized the order derivatives, using the obtained parameters and conditions. The grey curves depict their results and the black curve shows the best fit with an RMSD of 1762.13.

Figure 2 depicts the density of errors for the fitted parameters and order derivatives, categorized into integer and fractional orders, represented by the left and right sides of the violin plot, respectively. The results reveal that the mean and minimum errors of the model with fractional orders are comparatively lower than those of the model with integer orders. It highlights the enhanced flexibility and improved data fitting by incorporating fractional derivatives into the model.

The tables presenting the optimal values of the parameters, initial conditions, and order derivatives, along with their corresponding statistical properties such as mean, standard deviation, and median can be found in Table 2.

Table 2: Statistical Properties of Model Parameters: This table presents the mean, standard deviation, and median of model parameters, order derivatives, and initial conditions, alongside the sensitivity index for R_0 ($S_P^{R_0}$) considering optimized values within integer (ODE) and fractional order derivatives (FDE) models.

Parameters	Mean	STD	Median	Optimized value		Sensitivity	
				ODE	FDE	ODE	FDE
Λ	-	-	-	-	-	1.0000	1.0000
μ	-	-	-	-	-	-0.7109	-0.7115
μ_p	0.0038	0.0039	0.0026	0.0036	0.0023	-0.2657	-0.2657
ϕ_1	3.11e-6	1.32e-5	5.55e-7	8.15e-7	1.04e-6	0.0000	0.0000
ϕ_2	0.6341	0.2381	0.6711	0.4394	0.8344	0.0000	0.0000
β_1	1.32e-5	4.77e-5	2.94e-6	2.80e-6	2.32e-5	0.9964	0.7250
β_2	1.18e-6	1.20e-6	8.23e-7	8.86e-7	9.05e-7	0.8618	0.0025
δ	0.3270	0.0633	0.3335	0.4947	0.3880	-0.9737	-0.9757
ψ	0.0996	0.1703	0.0323	0.0002	0.0032	-0.0004	-0.0004
ω	0.4764	0.2060	0.4342	0.5396	0.7022	0.0173	0.0577
σ	0.0015	0.0005	0.0015	0.0012	0.0017	-0.0591	-0.0591
γ_S	0.0009	0.0007	0.0007	0.0701	0.0009	-0.0021	-0.0010
γ_A	0.0726	0.0112	0.0716	0.0001	0.0744	-0.0074	-0.0074
η_S	0.0065	0.0099	0.0030	0.0064	0.0007	0.0023	0.0014
η_A	0.4177	0.2867	0.3542	0.3585	0.0524	0.9941	0.9950
Order derivatives	Mean	STD	Median	Optimized value		Sensitivity	
α_S	1.0000	1.1e-16	1.0000	1.0000		0.7504	
α_E	0.9702	0.0157	0.9671	0.9591		-10.943	
α_{I_A}	0.9853	0.0530	1.0000	1.0000		4.4178	
α_{I_S}	0.8641	0.0783	0.8604	0.7868		0.0035	
α_R	0.7847	0.0776	0.7665	0.7000		0.0000	
α_D	0.7731	0.1171	0.7000	0.7018		0.0000	
α_W	0.9990	0.0090	1.0000	1.0000		4.6752	
Initial conditions	Mean	STD	Median	Optimized value			
$S(0)$	70088.0	16318.8	65858.9	57674.0		83379.9	
$E(0)$	0.81708	0.89169	0.57169	0.1181		0.1002	
$I_A(0)$	0.38595	0.47730	0.20705	0.1093		0.0404	
$W(0)$	0.64895	1.25392	0.30470	0.0015		1.0605	

4.1. Sensitivity analysis of the basic reproduction number

This section examines the influence of different factors on the transmission of epidemic diseases. Policymakers can make informed decisions regarding public health interventions by assessing the sensitivity of R_0 to various parameters, such as social distancing measures. Furthermore, this methodology allows for identifying parameters that have the most significant impact on disease propagation. To assess the effects of minor variations in a parameter or a derivative order, denoted both by \mathcal{P} , on the basic reproduction number R_0 , we introduce the forward normalized sensitivity index of R_0 for \mathcal{P} , which can be mathematically formulated as:

$$S_{\mathcal{P}}^{R_0} = \frac{\partial R_0}{\partial \mathcal{P}} \frac{\mathcal{P}}{R_0}.$$

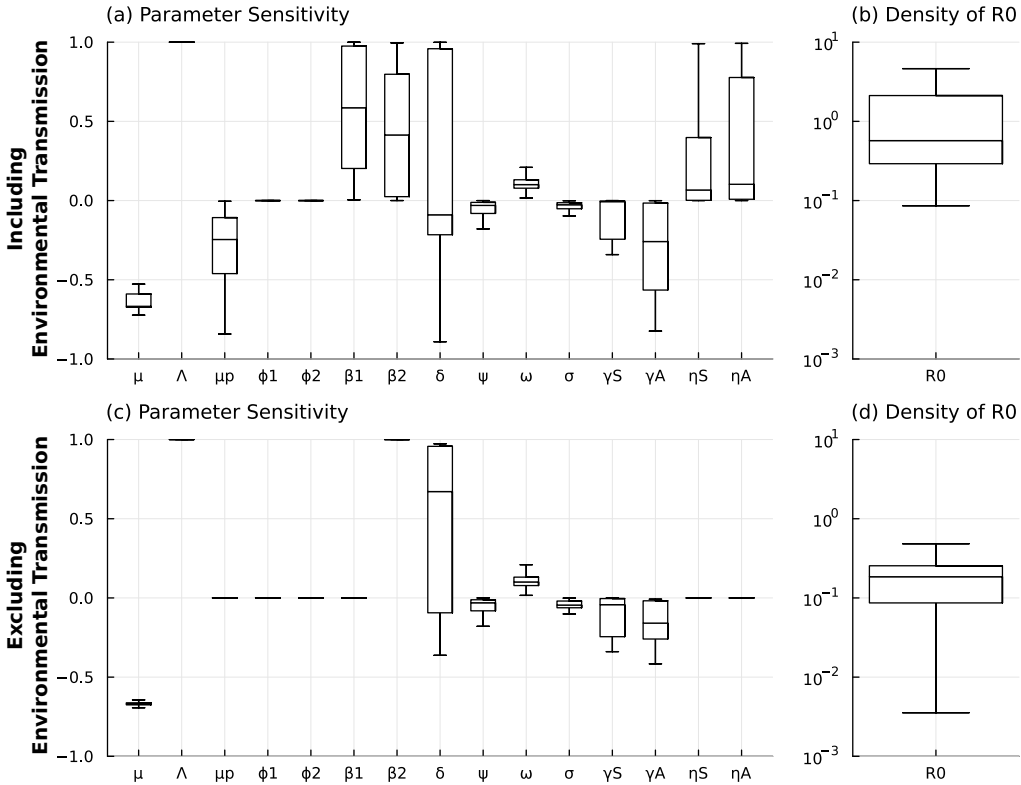


Figure 3: Sensitivity Analysis of R_0 for Model (1) with Integer Order Derivatives. (a) The boxplots of the sensitivity indices of R_0 to the parameter values, and (b) the distribution of R_0 for these values. (c) The sensitivity indices of R_0 to parameters when the environmental pathogen-related coefficients β_1 , η_S , and η_A are constrained to zero. (d) Illustration of the resulting influence on R_0 when the contributions of environmental transmission factors are eliminated.

If the sensitivity index of $S_{\mathcal{P}}^{R_0}$ is positive, it indicates an increase in the value of the basic reproduction number R_0 concerning \mathcal{P} . Conversely, the sensitivity index will be negative if the value of R_0 decreases in response to \mathcal{P} changes.

The computed sensitivity indices for R_0 to the optimized values have been demonstrated in Table 2. In addition, we illustrate the distribution of sensitivity indices of the parameters on R_0 through boxplots, together with the density of R_0 for these values in Figure 3(a-b), for the integer order model. Our analysis revealed that only the parameter δ , representing the proportion of symptomatic infectious individuals, mainly exhibited positive but sometimes negative sensitivity. In contrast, the other parameters maintained their sign of sensitivity indices.

Moreover, exploring the sensitivity of R_0 to parameters that facilitate virus transmission—specifically β_1 , η_S , and η_A —presents an interesting area of discussion. Notice that μ_P , representing

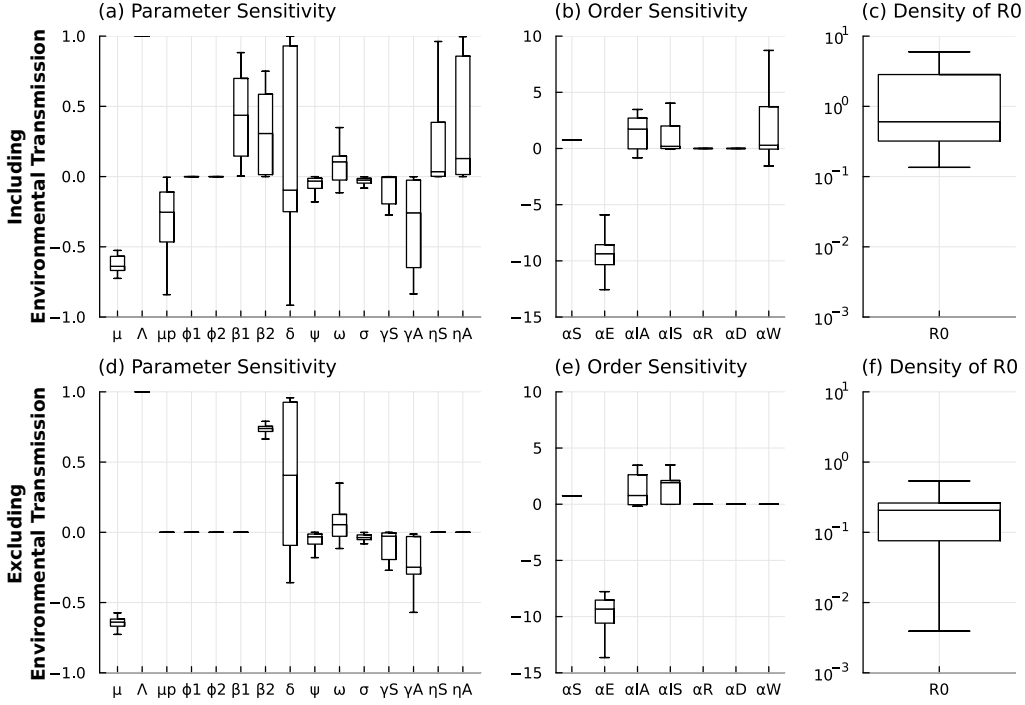


Figure 4: Sensitivity Analysis of R_0 for Model (1) with Fractional Order Derivatives. (a) The boxplots of the sensitivity indices of R_0 to the parameter values and (b) order derivatives, and (c) the distribution of R_0 for these values. (d) The sensitivity indices of R_0 to parameters and (e) order derivatives when the environmental pathogen-related coefficients β_1 , η_S , and η_A are constrained to zero. (f) Illustration of the resulting influence on R_0 when the contributions of environmental transmission factors are eliminated.

the natural death rate of the pathogen in the environment, is excluded from this analysis due to its consistently negative sensitivity index and it is beyond human control. Similarly, ϕ_1 is omitted as it does not feature in the equation (30) and thus has no impact on the sensitivity. In contrast, the sensitivity indices of β_1 , η_S , and η_A are positive, raising interesting considerations regarding the potential effects on R_0 through rigorous preventative measures, such as enhanced caution, hand washing, mask usage, and efforts to eliminate environmental contamination. Under these assumptions, the significant impact on R_0 is illustrated in Figure 3(c-d), demonstrating that R_0 could be reduced to below 1 with optimal interventions.

A particularly significant and intriguing aspect is the comparison of the impacts of fractional orders in sensitivity analysis. Figure 4(a) illustrates that in the fractional model, all parameters exhibit somewhat similar behaviors in terms of their sensitivity indices on R_0 when compared to the integer model. However, there are instances where ω may negatively influence R_0 . Figure 4(b) unveils the sensitivity of the order of derivatives on R_0 , which is noteworthy due to the challenging nature of interpreting the effects of orders on R_0 . Interestingly, it reveals that the sensitivity index of α_E is negative, whereas the indices for other orders are predominantly positive. This provides a preliminary insight into the impact of derivative orders on R_0 . It also results that R_0 values in fractional-order models are marginally higher than those in integer-order models, comparing Figure 4(c) with Figure 3(c). Furthermore, echoing the observations made with the integer model, Figure 4(d-f) also demonstrates how mitigating environmental transmission factors influences the outcomes in the fractional order model.

4.2. Numerical methods and implementation

The numerical analyses in this study were carried out using the Julia programming language. The FdeSolver.jl package (v 1.0.7) solves fractional differential equations, implementing predictor-corrector algorithms and product-integration rules [41]. Parameter estimation was

performed using Bayesian inference and Hamiltonian Monte Carlo (HMC) with the Turing.jl package, and ODEs were solved using the DifferentialEquations.jl package. The order of derivatives was optimized using the function (L)BFGS, which employs the (Limited-memory) Broyden–Fletcher–Goldfarb–Shanno algorithm from the Optim.jl package in combination with FdeSolver.jl.

In our efforts to derive parameters and orders, our goal is not merely to identify the optimal solutions, parameters, and orders, but rather to establish a reasonable range of values. This approach allows us to assess the impact of pathogen shedding in our modeling and to explore the influence of fractional derivatives within this context. However, this process necessitates certain considerations. For instance, we account for a coefficient representing the proportion of asymptomatic cases (I_A) that undergo COVID-19 testing (denoted by T), aiming for a more realistic evaluation of confirmed case data. This is based on the premise that data is predominantly derived from those who have been tested for COVID-19. Assuming that all symptomatic cases (I_S) and only a portion of I_A are tested, the confirmed cases are represented by $I_S + TI_A$. This adjustment introduces an additional equation to more accurately fit the recovered (R) compartment, acknowledging that records of recovery only include tested individuals from both I_A and I_S groups. It is important to note that while this modification does not alter the overall model or our analysis—since it involves independent equations—it enhances the realism of the fit.

Ultimately, one must recognize that the flexibility afforded by the fractional model does not inherently equate to a superior or more accurate fit, as it could potentially lead to overfitting. Therefore, further analysis, such as cross-validation, is essential, especially in scenarios where parameter values have significant implications for policy-making.

4.3. Data and code availability

All computational results for this article are available on GitHub and accessible via <https://github.com/moeinkh88/> including all data and code used for running the simulations and generating the figures.

5. Conclusion

In concluding the paper on the fractional model of COVID-19 transmission with environmental pathogens as a shedding effect, it is pertinent to encapsulate the significant contributions, findings, and potential implications for future research and policy-making. This paper has meticulously developed a fractional-order compartmental model, enhancing the conventional framework by incorporating environmental transmission vectors and accounting for asymptomatic and symptomatic infections. Through rigorous mathematical analysis, including existence, uniqueness, boundedness of solutions, and stability analyses, the model’s robust theoretical foundation has been solidly established.

Numerical results have significantly demonstrated the model’s utility in simulating the dynamics of COVID-19 transmission, highlighting a more flexible fit with actual data when fractional derivatives are employed, thus offering broader insight into the disease’s spread. The sensitivity analysis of the basic reproduction number R_0 has revealed critical parameters and order of derivatives influencing the transmission dynamics, guiding targeted interventions. The model has also highlighted the considerable impact of environmental transmission factors, suggesting that mitigating these can substantially lower R_0 , thereby controlling the outbreak’s spread.

This study emphasizes the importance of incorporating environmental factors and fractional calculus in modeling infectious diseases, offering a more comprehensive and flexible framework. Recognizing the combined and cross-disciplinary endeavor, this research sets a precedent for subsequent inquiries, encouraging the academic and scientific arenas to persist in evolving and refining mathematical models to confront infectious diseases more effectively in the future.

Declaration of Competing Interest

The authors declare no conflict of interest.

Acknowledgment

This study has been supported by the Academy of Finland (330887 to MK, LL), the European Union’s Horizon 2020 research and innovation program (952914 to LL), and the UTUGS graduate school of the University of Turku (to MK).

The authors wish to acknowledge CSC–IT Center for Science, Finland, for computational resources.

References

- [1] Faiçal Ndaïrou, Iván Area, Juan J. Nieto, and Delfim F.M. Torres. Mathematical modeling of covid-19 transmission dynamics with a case study of wuhan. *Chaos, Solitons & Fractals*, 135:109846, 2020.
- [2] Sebastien Boyer, Borin Peng, Senglong Pang, Véronique Chevalier, Veasna Duong, Christopher Gorman, Philippe Dussart, Didier Fontenille, and Julien Cappelle. Dynamics and diversity of mosquito vectors of japanese encephalitis virus in kandal province, cambodia. *Journal of Asia-Pacific Entomology*, 23(4):1048–1054, 2020.
- [3] Muhammad Altaf Khan, Yasir Khan, and Saeed Islam. Complex dynamics of an seir epidemic model with saturated incidence rate and treatment. *Physica A: Statistical mechanics and its applications*, 493:210–227, 2018.
- [4] Xingbo Liu and Lijuan Yang. Stability analysis of an seiqv epidemic model with saturated incidence rate. *Nonlinear Analysis: Real World Applications*, 13(6):2671–2679, 2012.
- [5] Swati and Nilam. Fractional order sir epidemic model with beddington–de angelis incidence and holling type ii treatment rate for covid-19. *Journal of Applied Mathematics and Computing*, 68(6):3835–3859, Dec 2022.
- [6] Chunyan Ji. The threshold for a stochastic hiv-1 infection model with beddington-deangelis incidence rate. *Applied Mathematical Modelling*, 64:168–184, 2018.
- [7] Adnane Boukhouima, Khalid Hattaf, and Noura Yousfi. Dynamics of a fractional order hiv infection model with specific functional response and cure rate. *International Journal of Differential Equations*, 2017:8372140, Aug 2017.
- [8] El Mehdi Lotfi, Mehdi Maziane, Khalid Hattaf, and Noura Yousfi. Partial differential equations of an epidemic model with spatial diffusion. *International Journal of Partial Differential Equations*, 2014:186437, Feb 2014.
- [9] Iván Area, Francisco J Fernández, Juan J Nieto, and F Adrián F Tojo. Concept and solution of digital twin based on a stieltjes differential equation. *Mathematical Methods in the Applied Sciences*, 45(12):7451–7465, 2022.
- [10] Samuel Mwalili, Mark Kimathi, Viona Ojiambo, Duncan Gathungu, and Rachel Mbogo. Seir model for covid-19 dynamics incorporating the environment and social distancing. *BMC Research Notes*, 13(1):1–5, 2020.
- [11] Anuraj Singh and Preeti Deolia. Covid-19 outbreak: a predictive mathematical study incorporating shedding effect. *Journal of Applied Mathematics and Computing*, 69(1):1239–1268, 2023.
- [12] Salisu M Garba, Jean M-S Lubuma, and Berge Tsanou. Modeling the transmission dynamics of the covid-19 pandemic in south africa. *Mathematical biosciences*, 328:108441, 2020.
- [13] Faiçal Ndaïrou and Delfim F. M. Torres. Mathematical analysis of a fractional covid-19 model applied to wuhan, spain and portugal. *Axioms*, 10(3), 2021.

- [14] Faiçal Ndairou, Iván Area, Juan J. Nieto, Cristiana J. Silva, and Delfim F.M. Torres. Fractional model of covid-19 applied to galicia, spain and portugal. *Chaos, Solitons & Fractals*, 144:110652, 2021.
- [15] Meghdad Saeedian, Moein Khalighi, Nahid Azimi-Tafreshi, Gholamreza Jafari, and Marcel Ausloos. Memory effects on epidemic evolution: The susceptible-infected-recovered epidemic model. *Physical Review E*, 95:022409, 2017.
- [16] Faiçal Ndairou, Moein Khalighi, and Leo Lahti. Ebola epidemic model with dynamic population and memory. *Chaos, Solitons & Fractals*, 170:113361, 2023.
- [17] Faiçal Ndairou, Moein Khalighi, and Leo Lahti. Ebola epidemic model with dynamic population and memory. *Chaos, Solitons & Fractals*, 170:113361, 2023.
- [18] Hadi Jahanshahi, Jesus M. Munoz-Pacheco, Stelios Bekiros, and Naif D. Alotaibi. A fractional-order sird model with time-dependent memory indexes for encompassing the multi-fractional characteristics of the covid-19. *Chaos, Solitons & Fractals*, 143:110632, 2021.
- [19] Kai Diethelm. A fractional calculus based model for the simulation of an outbreak of dengue fever. *Nonlinear Dynamics*, 71:613–619, 2013.
- [20] Lazarus Kalvein Beay and Nursanti Anggriani. Dynamical analysis of a modified epidemic model with saturated incidence rate and incomplete treatment. *Axioms*, 11(6), 2022.
- [21] Yanan Zhao and Daqing Jiang. The threshold of a stochastic sirs epidemic model with saturated incidence. *Applied Mathematics Letters*, 34:90–93, 2014.
- [22] Xiangyun Shi, Xueyong Zhou, and Xinyu Song. Dynamical behavior of a delay virus dynamics model with ctl immune response. *Nonlinear Analysis: Real World Applications*, 11(3):1795–1809, 2010.
- [23] Dan Li and Wanbiao Ma. Asymptotic properties of a hiv-1 infection model with time delay. *Journal of Mathematical Analysis and Applications*, 335(1):683–691, 2007.
- [24] Oyoon Abdul Razzaq, Najeeb Alam Khan, Muhammad Faizan, Asmat Ara, and Saif Ullah. Behavioral response of population on transmissibility and saturation incidence of deadly pandemic through fractional order dynamical system. *Results in Physics*, 26:104438, 2021.
- [25] Igor Podlubny. *Fractional differential equations: An introduction to fractional derivatives, fractional differential equations, to methods of their solution and some of their applications*. Elsevier, 1998.
- [26] Anatoly Aleksandrovich Kilbas, Hari M Srivastava, and Juan J Trujillo. *Theory and applications of fractional differential equations*, volume 204. Elsevier, 2006.
- [27] Hamed Al-Sulami, Moustafa El-Shahed, Juan J Nieto, and Wafa Shammakh. On fractional order dengue epidemic model. *Mathematical Problems in Engineering*, 2014:1–6, 2014.
- [28] Yu-Ming Chu, Saima Rashid, Ahmet OcaK Akdemir, Aasma Khalid, Dumitru Baleanu, Bushra R. Al-Sinan, and O.A.I. Elzibar. Predictive dynamical modeling and stability of the equilibria in a discrete fractional difference covid-19 epidemic model. *Results in Physics*, 49:106467, 2023.
- [29] Zaid M. Odibat and Nabil T. Shawagfeh. Generalized taylor’s formula. *Applied Mathematics and Computation*, 186(1):286–293, 2007.
- [30] Kai Diethelm, Ha Duc Thai, and Hoang The Tuan. Asymptotic behaviour of solutions to non-commensurate fractional-order planar systems. *Fractional Calculus and Applied Analysis*, 25(4):1324–1360, 2022.

- [31] Pauline Van den Driessche and James Watmough. Reproduction numbers and sub-threshold endemic equilibria for compartmental models of disease transmission. *Mathematical Biosciences*, 180(1):29–48, 2002.
- [32] Yan Li, YangQuan Chen, and Igor Podlubny. Stability of fractional-order nonlinear dynamic systems: Lyapunov direct method and generalized mittag–leffler stability. *Computers & Mathematics with Applications*, 59(5):1810–1821, 2010. Fractional Differentiation and Its Applications.
- [33] E. Ahmed and A.S. Elgazzar. On fractional order differential equations model for nonlocal epidemics. *Physica A: Statistical Mechanics and its Applications*, 379(2):607–614, 2007.
- [34] A.E. Matouk. Stability conditions, hyperchaos and control in a novel fractional order hyperchaotic system. *Physics Letters A*, 373(25):2166–2173, 2009.
- [35] J.P LaSalle. Stability theory for ordinary differential equations. *Journal of Differential Equations*, 4(1):57–65, 1968.
- [36] Soon-Mo Jung. *Hyers-Ulam-Rassias stability of functional equations in nonlinear analysis*, volume 48. Springer Science & Business Media, 2011.
- [37] Dumitru Baleanu Isa Abdullahi Baba. Awareness as the most effective measure to mitigate the spread of covid-19 in nigeria. *Computers, Materials & Continua*, 65(3):1945–1957, 2020.
- [38] Ensheng Dong, Hongru Du, and Lauren Gardner. An interactive web-based dashboard to track covid-19 in real time. *The Lancet Infectious Diseases*, 20(5):533–534, 2020.
- [39] Calistus N. Ngonghala, Enahoro Iboi, Steffen Eikenberry, Matthew Scotch, Chandini Raina MacIntyre, Matthew H. Bonds, and Abba B. Gumel. Mathematical assessment of the impact of non-pharmaceutical interventions on curtailing the 2019 novel coronavirus. *Mathematical Biosciences*, 325:108364, 2020.
- [40] Neil M Ferguson, Daniel Laydon, Gemma Nedjati-Gilani, Natsuko Imai, Kylie Ainslie, Marc Baguelin, Sangeeta Bhatia, Adhiratha Boonyasiri, Zulma Cucunubá, Gina Cuomo-Dannenburg, et al. Report 9: Impact of non-pharmaceutical interventions (npis) to reduce covid19 mortality and healthcare demand. 16, 2020.
- [41] Moein Khalighi, Giulio Benedetti, and Leo Lahti. Fdesolver: A julia package for solving fractional differential equations. *arXiv:2212.12550*, 2022.